Experimental Evidence for a New Parameter to Control the Glass Transition of Confined Polymers

S. Srivastava and J. K. Basu*

Department of Physics, Indian Institute of Science, Bangalore 560 012, India

(Received 22 December 2006; published 20 April 2007)

Polymer nanocomposites can be used to study confinement effects on the polymer glass transition temperature (T_g) in a controlled manner by varying interparticle spacing. Using gold nanoparticles in polymethylmethacrylate, we show how the polymer T_g can be tuned by variation of the nanoparticle-polymer interface width (σ), keeping interparticle spacing fixed. We report the first experimental observation of a crossover in the sign of T_g deviation for confined polymers by variation of σ and propose a model to explain the dependence of crossover width on the spatial extent of cooperatively rearranging regions.

DOI: 10.1103/PhysRevLett.98.165701 PACS numbers: 64.70.Pf, 61.10.Eq, 61.41.+e, 61.46.−w

Finite size effects on the glass transition of polymers has been one of the most widely studied areas of condensed matter physics [1,2]. The glass transition temperature T_g of confined polymers shows both positive and negative deviation, due to a combination of confinement and surface effects [1–8]. Experiments have been motivated by the possibility to detect a spatial correlation length corresponding to a cooperatively rearranging region (CRR) ξ associated with the glass transition, by tuning the length scale of confinement to ξ. The existence of such a length scale has been predicted by the phenomenological Adams-Gibbs model [9] whereby the onset of glass transition gives rise to cooperatively molecular motion within regions of size ξ. Recent simulations [10,11] and experiments [12,13] have also provided evidence of cooperative and heterogeneous dynamics and an associated length scale in various types of liquids including polymers, although the precise connection between the two is still an open question. Experiments on glass transition of confined liquids have failed to provide unambiguous evidence for the existence of such a length scale due to the controversial nature of available results [1,2,4–7]. This is largely because in the various experimental systems used to study finite size effects, like cavities and pores [14], thin films [3–7,15,16], and nanoparticle-embedded glasses [8,17–20], T_g is affected not only by confinement but also due to surface effects [2–8,17–20]. The role of surface and interface on T_g of confined polymers has recently been investigated in various experiments on thin polymer films [3–7]. A phenomenological model was also proposed by de Gennes [21] to suggest the existence of a surface layer in polymer films with higher mobility, as compared to bulk, due to reduction of entanglement. Recent simulations have also pointed to the role of surface morphology in dictating not only the magnitude but the sign of T_g deviation as well [2,22–24]. It is evident from recent experiments [8,17–19] on polymer nanocomposites that T_g decreases with increasing volume fraction of embedded nanoparticles for a noninteracting particle-polymer interface while it increases for attractive interactions. However, it is not clear whether there is a possibility of a change in the sign of T_g shift, for the same polymer-particle interaction (repulsive or attractive). Evidence for the existence of interfacial layers has also been presented for polymer nanocomposites [20] although neither an ability to control this surface layer nor a clear understanding of how this affects polymer T_g has been demonstrated. The advantage of polymer nanocomposites is the possibility to control various parameters, such as average interparticle spacing h, polymer-nanoparticle interactions, and interface morphology in tuning the thermomechanical properties of polymers, in general, and their glass transition, in particular. The major challenge in effective utilization of polymer nanocomposites, though, is to obtain a homogeneous dispersion of the nanoparticles within a polymer matrix [8,18,25]. In order to have a homogeneously dispersed nanoparticle-polymer composite system with controllable interface morphology, we have synthesized gold nanoparticles of various sizes (6–20 nm) capped with polymethylmethacrylate (PMMA) and embedded in the same polymer matrix.

In situ synthesis of gold nanoparticles in the presence of PMMA (molecular weight 120 K, Sigma-Aldrich) was carried out by the reduction of a $HAuCl_4$ (Sigma-Aldrich) solution in ethanol (Merck), with freshly prepared aqueous (18.2 MΩ, Barnstead) solution of $NaBH_4$ (Sigma-Aldrich), using some modifications to a method used in [26]. The concentration of capping PMMA was varied by a factor of ~15 to obtain gold nanoparticles of various sizes. On addition of $NaBH_4$ solution, the color of the $HAuCl_4$ solution instantaneously changed from yellow to brownish red, indicating the formation of gold nanoparticles which were stable for several months. Formation of stable gold nanoparticles in solution was further confirmed from ultraviolet-visible (UV-Vis) spectroscopy (Fig. 1). The size and polydispersity of the PMMA-capped nanoparticles were quantitatively estimated from transmission electron microscopy (TEM) images of nanoparticles. To prepare nanoparticle-embedded polymer composites the

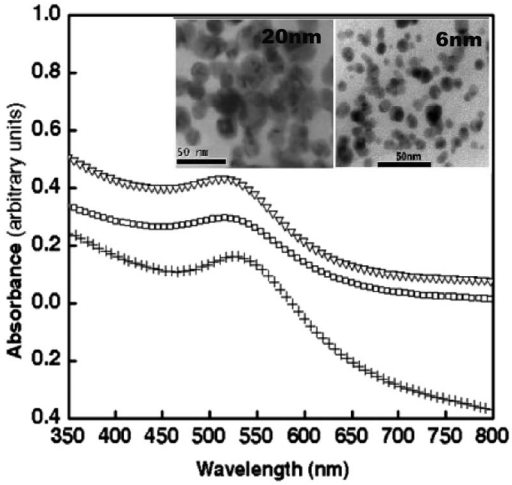

FIG. 1. UV-Vis absorption spectra of gold nanoparticles in aqueous ethanol solution, with diameters of 6 nm (square), 14 nm (triangle), and 20 nm (plus). Inset: TEM images of gold nanoparticles of diameter 6 ± 1 nm and 20 ± 3 nm in PMMA.

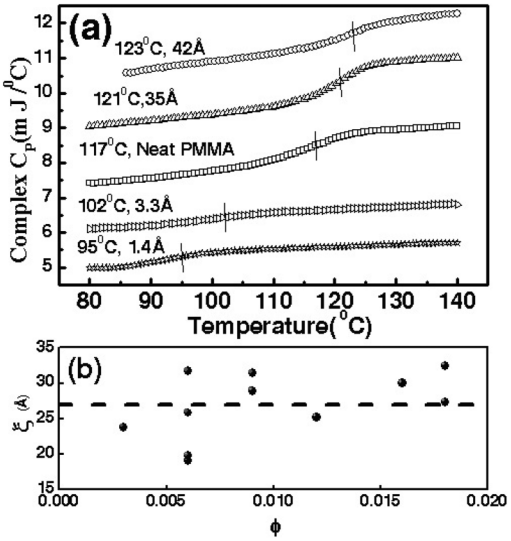

FIG. 2. (a) Complex specific heat for neat PMMA and several gold nanoparticle-embedded PMMA nanocomposites. Indicated numbers are (T_g, σ). (b) The size of CRR ξ at different volume fractions φ of gold nanoparticles in a PMMA matrix. The dashed line indicates the mean ξ.

respective powders were obtained after addition of the required amount of PMMA to the gold nanoparticles in either a good (acetone, toluene) or a bad solvent (acetone: water, 1:10). The color of the powders obtained by controlled evaporation does not change significantly from that of the solution, indicating the absence of major particle aggregation. We were able to readily disperse these gold nanoparticles of different sizes into a PMMA matrix at various fractions from 0.002–0.08. Modulated differential scanning calorimetry (MDSC) measurements (TA Instrument) were used to characterize the glass transition of polymer nanocomposites, as described below. Initial heating up to 150 °C followed by cooling down to 50 °C; heating at a constant underlying rate of 3 °C/ min up to 150 °C; cooling at the same rate down to 50 °C; reheating at the same rate up to 150 °C with modulation period of 100 sec and amplitude of 1 °C followed by modulated cooling down to 50 °C. The measurements on all the samples were repeated under identical conditions, at different times, and only the reproducible data sets were used in our analysis. Conditions for reproducibility were assessed by measurements on PMMA and other polymer standards.

The large range of T_g observed, as shown in Fig. 2(a), is quite remarkable for a particular type of polymer-particle interaction. More significantly, we see both an increase and a decrease of T_g with respect to the neat PMMA. We have used this data to also estimate the value of ξ, using the following equation [27],

$$\xi^2 = \frac{k_B T^2 (1/C_V^2)(\partial C_V/\partial T)}{\rho \Delta T^2}. \quad (1)$$

Here, ΔT and ΔC_v are the width of the glass transition region and the magnitude of change in specific heat across the transition region, respectively, ρ is the density of polymer, T is T_g, and k_B is the Boltzmann constant. It was found that for all the nanocomposite samples ξ varied from 25–30 Å (Fig. 2(b)), which is typical of PMMA.

As has been indicated earlier [8,18,19,25], nanoparticle-polymer interface morphology plays a crucial role in determining the thermomechanical properties of polymer nanocomposites. We have used small angle x-ray scattering (SAXS), a widely used technique [28–30] to determine interface morphology, to characterize our polymer nanocomposite samples. SAXS data were collected on a Kratky collimation based system (Hecus) coupled to a sealed tube generator. All measurements were performed under vacuum with Ni filter on the incident side to ensure monochromatic Cu-K_α (wavelength $\lambda = 1.54$ Å) radiation with a wide open slit height of 10 mm, to ensure complete desmearing, and width of 250 μm, at a fixed sample to detector [one dimensional position sensitive detector with pixel size of 54 μm] distance of 268 mm. For data collection the samples were sandwiched between two mica sheets of known thickness and background were subtracted from blank mica sheets.

It is well known that in the high q [$= (4\pi \sin\theta/\lambda)$, 2θ is the scattering angle] Porod region of a SAXS scattering curve the intensity decays as [28–30] $I_{q\to\infty} \propto K/q^{4+\alpha}$ ($I'_{q\to\infty} \propto K'/q^{3+\alpha}$ for slit smeared data, where K is the Porod constant, $K' \sim \pi K/2$, and I' represents the smeared intensity). Depending on the value of this exponent α interface can be fractally rough ($\alpha < 0$), smooth ($\alpha = 0$), or diffuse ($\alpha > 0$). The slopes were determined by linear fits in the Porod region. For all the analysis presented here, to estimate the exponent α, scattering intensity multiplied by q^3 was used. It has been verified that within the error bars the value of α extracted from smeared ($q^3 I$) and

desmeared ($q^4 I$), smoothed, data are identical. Hence the smeared data have been used for analysis. From Porod analysis of SAXS data, shown in Fig. 3(a), we found that $\alpha > 0$, indicating a diffuse gold-PMMA interface. The interfacial width σ is proportional to α, and various methods [29,30] can be used to extract this width numerically from the measured exponent. However, the best fit to the deviation from Porod law turned out to be power law also, for which no standard method exists to extract the real space interface density profile analytically. Hence we have used numerical fast Fourier transform (FFT) of the power law decay in the Porod region to extract the real space density profile, as shown in Fig. 3(b). To check the consistency of the inversion scheme we have generated scattering curves with different types of interface density profiles, like linear and exponential, and found that our numerical FFT scheme does indeed give the same width for the above profiles, within numerical errors.

In the inset of Fig. 3(b) we have also shown the dependence of σ on the parameter φ_{poly}/R that, in some ways, represents the surface density of adsorbed PMMA chains on gold nanoparticles. Here φ_{poly} is the polymer concentration and R is the radius of the gold nanoparticle. However, this is a subtle point since σ does not depend merely on the surface density of adsorbed chains but more specifically on the surface segmental density, which, apart from the chain density, also depends crucially on the solvent conditions, as discussed later.

We first discuss the confinement effects visible for our polymer nanocomposite systems. The average interparticle spacing, $h = 2(\sqrt[3]{\varphi_p/\varphi} - 1)R$, can be calculated using the known volume fraction φ of gold nanoparticles, assuming a maximum random packing fraction of $\varphi_p = 0.638$. Here, h plays the role of a confinement parameter, as in thin films or pores, and polymer segments are confined between neighboring nanoparticles. For systems showing negative deviation of T_g, ΔT_g is found to increase with a decrease in interparticle spacing h [Fig. 4(a), lower panel]. Similar trends are found for systems exhibiting positive deviation [Fig. 4(a) (upper panel)], although this behavior is not expected for gold-PMMA nanocomposites. The negative deviation of T_g can be explained in terms of confinement effect. Fourier transform infrared spectra of neat PMMA and PMMA embedded with gold nanoparticles of various sizes and fractions are almost identical, indicating very weak PMMA-gold interaction. For such nonattractive polymer-surface interaction, it is expected that with decrease in h, the confinement effects will become increasingly prominent, leading also to a decrease in T_g. The observed behavior of T_g shift seems to be consistent with earlier observations, but the positive T_g deviation cannot be explained. There seems to be a clear crossover region [Fig. 4(b)] in the interface width ($\sigma_c \sim 26$ Å) below which ΔT_g is negative while above it, it is positive. Hence it is clear from the above discussion that the interface morphology can determine the sign of ΔT_g for polymers under confinement.

To explain this observation we need to examine, more closely, the role played by nanoparticle-polymer surface

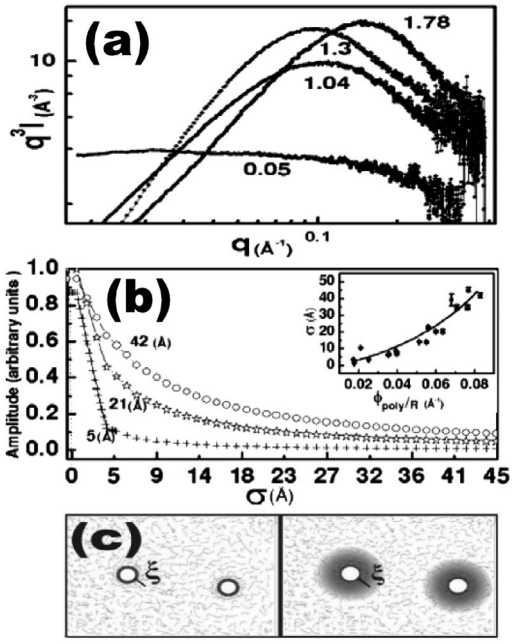

FIG. 3. (a) Porod plot of SAXS data. The value of α in the Porod region for the respective data on several nanocomposite samples is indicated alongside each profile. (b) Corresponding interface density profile. Inset: σ vs φ_{poly}/R. (c) Schematic explaining our model for T_g deviation based on the relative values of σ (indicated by the shaded region around nanoparticles) and ξ, (solid line) in extreme cases of $\sigma \ll \xi$ (left panel) and $\sigma \gg \xi$ (right panel).

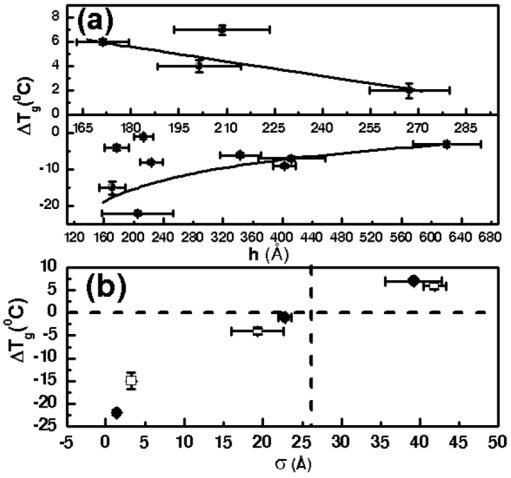

FIG. 4. (a) Effect of interparticle spacing h on ΔT_g ($\Delta T_g = T_{g(\text{nanocomp})} - T_{g(\text{PMMA})}$). Upper panel: positive ΔT_g. Lower panel: negative ΔT_g. (b) ΔT_g vs σ for fixed values of h, 174 ± 3 Å (squares) and 209 ± 3 Å (filled circles) clearly showing the surface morphology effect at fixed confinement. Crossover from negative to positive ΔT_g occurs at $\sim\sigma_c$ (vertical dashed line).

morphology, specifically interfacial width σ. The main parameters controlling σ, in our polymer nanocomposites, are the capping polymer concentration in solution and the solvent used to prepare the composites, as shown clearly in the inset of Fig. 3(b). Generally, σ increases with an increase in polymer concentration for a given type of solvent, and larger interfacial widths are obtained for bad solvents than for good solvents at same φ_{poly}. We propose a model, based on our experimental observations, to provide a microscopic understanding of the physics relating the nanoparticle-polymer interface morphology to the observed crossover in the sign of T_g deviation in polymer nanocomposites, which should also be valid, in general, for polymers under all forms of confinement. Two competing effects—modification of polymer segmental mobility due to decrease in entropy at the surface and reduction in mobility due to enhancement of interface segmental density [2,22,23,31] above that of the bulk—come into play at the nanoparticle-polymer interface in determining segmental relaxation times and hence the T_g. As has been discussed earlier, the Adams-Gibbs model of the glass transition envisages existence of a growing spatial correlation length within a glass former with decreasing temperature from above T_g, within which molecular motion is correlated. For the case of the polymer nanocomposites, this correlated segmental motion occurs within an approximate distance ξ [see Fig. 3(c)] away from nanoparticle-polymer interface. Simulations [2,22–24] have shown that the relaxation time of segments can be significantly different from the bulk value at the surface and the segmental relaxation time approaches the bulk value within a finite spatial extent from the nanoparticle surface, depending on the interaction and segmental density. Hence the mean T_g is decided by the average of the distribution of relaxation times within a layer spatial extent ξ. For small σ ($\sigma \ll \xi$) the interface is very sharp, as shown schematically in Fig. 3(c) (left panel), and the segmental density decays to that of bulk PMMA very fast, implying that the mean relaxation is dominated by that of the surface layer, which in our case is expected to be enhanced due to the nonattractive nature of the gold-PMMA interface, and hence a consequent reduction of T_g. For the other extreme of large σ ($\sigma \gg \xi$) the interface is very diffuse [Fig. 3(c) (right panel)] and there is enhancement of segmental density, even for our nonattractive interface, as has been found earlier [2,22–24]. In this case the mean interface segmental relaxation is dominated by slower relaxation of segments located farther away from the interface and overcompensates the higher mobility of segments, close to the interface, leading to an enhancement of T_g. For $\sigma \sim \xi$, $\Delta T_g \sim 0$ and the two effects cancel each other.

We have shown here how the glass transition of polymers can be tuned in a controlled fashion by embedding nanoparticles which have been coated with an identical polymer to control their interface morphology. Our results point to the extensive experimental, simulation, and theoretical work necessary to elucidate the role of interfacial effects on the glass transition of polymers under confinement and a careful interpretation of experiments on finite size effects. In turn this should also enable a better understanding of intrinsic finite size and surface effects on polymer glass transition.

We thank ISRO-IISc, Space Technology Cell, for financial support to carry out our research and DST-IISc Nanoscience Initiative for use of the TEM.

*Electronic address: basu@physics.iisc.ernet.in

[1] M. Alcoutlabi and G. B. McKenna, J. Phys. Condens. Matter **17**, R461 (2005).
[2] J. Baschanagel and F. Varnik, J. Phys. Condens. Matter **17**, R851 (2005).
[3] R. D. Priestley *et al.*, Science **309**, 456 (2005).
[4] H. Kim *et al.*, Phys. Rev. Lett. **90**, 068302 (2003).
[5] P. A. O'Connell and G. B. McKenna, Science **307**, 1760 (2005).
[6] J. A. Forrest, K. Dalnoki-Veress, J. R. Stevens, and J. R. Dutcher, Phys. Rev. Lett. **77**, 2002 (1996).
[7] S. Kawana and R. A. L. Jones, Phys. Rev. E **63**, 021501 (2001).
[8] A. Bansal *et al.*, Nat. Mater. **4**, 693 (2005).
[9] G. Adams and J. H. Gibbs, J. Chem. Phys. **43**, 139 (1965).
[10] C. Bennemann *et al.*, Nature (London) **399**, 246 (1999).
[11] S. Whitelam, L. Berthier, and J. P. Garrahan, Phys. Rev. Lett. **92**, 185705 (2004).
[12] E. V. Russell and N. E. Israeloff, Nature (London) **408**, 695 (2000).
[13] L. Berthier *et al.*, Science **310**, 1797 (2005).
[14] C. L. Jackson and G. B. Mckenna, J. Non-Cryst. Solids **131**, 221 (1991).
[15] J. L. Keddie, R. A. L. Jones, and R. A. Cory, Europhys. Lett. **27**, 59 (1994).
[16] Z. Fakhraai and J. A. Forrest, Phys. Rev. Lett. **95**, 025701 (2005).
[17] R. A. Narayanan *et al.*, Phys. Rev. Lett. **97**, 075505 (2006).
[18] Q. P. Joseph *et al.*, J. Polym. Sci., Part B: Polym. Phys. **41**, 3339 (2003).
[19] J. A. Benjamin, R. W. Seiegel, and L. S. Schadler, J. Polym. Sci., Part B: Polym. Phys. **42**, 4371 (2004).
[20] J. Berriot *et al.*, Europhys. Lett. **64**, 50 (2003).
[21] P. G. de Gennes, Eur. Phys. J. E **2**, 201 (2000).
[22] F. W. Starr, T. B. Schroder, and S. C. Glotzer, Macromolecules **35**, 4481 (2002).
[23] J. B. Hopper and K. S. Schweizer, Macromolecules **38**, 8858 (2005).
[24] P. Schiedler, W. Kob, and K. Binder, J. Phys. Chem. B **108**, 6673 (2004).
[25] A. C. Balazs, T. Emrick, and T. P. Russell, Science **314**, 1107 (2006).
[26] F. K. Liu *et al.*, Jpn. J. Appl. Phys. **42**, 4147 (2003).
[27] E. J. Donth, *The Glass Transition* (Springer, Berlin, 2001).
[28] S. K. Sinha *et al.*, Phys. Rev. B **38**, 2297 (1988).
[29] G. Tyagi, J. E. Mcgrath, and G. L. Wilkes, Polym. Eng. Sci. **26**, 1371 (1986).
[30] P. W. Schmidt, J. Chem. Phys. **94**, 1474 (1991).
[31] O. H. Seeck *et al.*, Europhys. Lett. **60**, 376 (2002).